JVI Journals.ASM.org

Temporal- and Strain-Specific Host MicroRNA Molecular Signatures Associated with Swine-Origin H1N1 and Avian-Origin H7N7 Influenza A Virus Infection

Emma-Kate Loveday,[a] Victoria Svinti,[a] Sandra Diederich,[a]* John Pasick,[b] and François Jean[a]

Department of Microbiology and Immunology, University of British Columbia, Vancouver, British Columbia, Canada,[a] and Canadian Food Inspection Agency, Winnipeg, Manitoba, Canada[b]

MicroRNAs (miRNAs) repress the expression levels of genes by binding to mRNA transcripts, acting as master regulators of cellular processes. Differential expression of miRNAs has been linked to virus-associated diseases involving members of the *Hepacivirus*, *Herpesvirus*, and *Retrovirus* families. In contrast, limited biological and molecular information has been reported on the potential role of cellular miRNAs in the life cycle of influenza A viruses (infA). In this study, we hypothesize that elucidating the miRNA expression signatures induced by low-pathogenicity swine-origin infA (S-OIV) pandemic H1N1 (2009) and highly pathogenic avian-origin infA (A-OIV) H7N7 (2003) infections could reveal temporal and strain-specific miRNA fingerprints during the viral life cycle, shedding important insights into the potential role of cellular miRNAs in host-infA interactions. Using a microfluidic microarray platform, we profiled cellular miRNA expression in human A549 cells infected with S- and A-OIVs at multiple time points during the viral life cycle, including global gene expression profiling during S-OIV infection. Using target prediction and pathway enrichment analyses, we identified the key cellular pathways associated with the differentially expressed miRNAs and predicted mRNA targets during infA infection, including the immune system, cell proliferation, apoptosis, cell cycle, and DNA replication and repair. By identifying the specific and dynamic molecular phenotypic changes (microRNAome) triggered by S- and A-OIV infection in human cells, we provide experimental evidence demonstrating a series of temporal and strain-specific host molecular responses involving different combinatorial contributions of multiple cellular miRNAs. Our results also identify novel potential exosomal miRNA biomarkers associated with pandemic S-OIV and deadly A-OIV-host infection.

MicroRNAs (miRNAs) are small endogenous, noncoding RNAs that are highly conserved and that have been recognized as a powerful tool for regulating gene expression through the RNA interference pathway (1, 2). The human genome encodes more than 1,000 miRNAs (miRBase v.16) that play key roles in diverse regulatory pathways, forming a complex network that is predicted to regulate more than 50% of protein coding genes (3). With the ability of one miRNA to bind and regulate numerous mRNAs and the potential for a single mRNA to be targeted by multiple miRNAs, it is possible to fine-tune the expression of proteins within the cell in a very precise manner (38). The deregulation of miRNA expression profoundly alters the gene expression in the cell and has been associated with many human pathologies (65).

In the case of viral infections, altered miRNA expression can be beneficial and/or detrimental to the viral life cycle, and it can also influence disease progression and outcome (14, 55). Human DNA viruses, most notably the herpesviruses, encode more than 200 viral miRNAs that can control viral gene expression and modulate cellular gene expression to allow for immune evasion and the establishment of latency (14, 55). For the human RNA viruses such as hepatitis C virus (HCV) and human immunodeficiency virus type 1 (HIV-1), modulation of host miRNAs influences viral pathogenesis (14). Throughout HCV infection, a liver-specific miRNA, miR-122, increases the accumulation and translation of HCV RNA by binding to the 5′-untranslated region (5′UTR) of the virus genome (20, 29, 31, 32). During HIV-1 infection, cellular miRNAs expressed in resting $CD4^+$ T lymphocytes were shown to negatively impact viral protein production and possibly contribute to HIV-1 latency, while miR-29a has been shown to directly target HIV-1 mRNAs leading to accumulation of viral mRNA at P-bodies for translational suppression (24, 47). Viruses also modulate the stability of host miRNA levels in order to interfere with host-cell gene expression. Such is the case with the noncoding uridine-rich RNA HSUR1 produced by herpesvirus saimiri, which has been shown to base pair extensively with the cellular miR-27, resulting in reduced stability and decreased levels of this miRNA within virally transformed T cells (6). Most recently, it was demonstrated that miR-141 was induced upon enterovirus 71 (EV71) infection and found to target eukaryotic translation initiation factor 4E (eIF4E), a key element in cap-dependent translation. Antagonizing miR-141 during EV71 infection dramatically reduced virus production, suggesting that expression of this cellular miRNA is important for the virus life cycle (22).

In contrast, the available research to date provides limited information on the role that miRNAs play during infection with

Received 29 November 2011 Accepted 8 March 2012
Published ahead of print 21 March 2012
Address correspondence to François Jean, fjean@mail.ubc.ca.
* Present address: Canadian Food Inspection Agency, Winnipeg, Manitoba, Canada.
E.-K.L. and V.S. contributed equally to this article.
Supplemental material for this article may be found at http://jvi.asm.org/.
Copyright © 2012, American Society for Microbiology. All Rights Reserved.
doi:10.1128/JVI.06892-11

influenza A viruses (infA). A microarray study of miRNA expression in mice during infection with the reconstructed 1918 (r1918) H1N1 virus and a seasonal H1N1 virus (Tx/91) was the first to report that the microRNAome was modulated during infA infection (36). Subsequent work on the highly pathogenic avian H5N1 infA strain, which can result in severe disease characterized by a systemic, rather than local, infection and major cytokine deregulation, further suggests that infA of various pathogenicities elicit distinct miRNA expression patterns during infection (34, 37).

In the present study, we hypothesize that elucidating the miRNA expression signatures induced by pandemic swine-origin infA (S-OIV) pandemic H1N1 (2009) and avian-origin infA (A-OIV) H7N7 (2003) associated with multiple cases of conjunctivitis and one case of acute respiratory distress syndrome in humans (10) could reveal temporal and strain-specific miRNA fingerprints during the viral life cycle. Using a high-throughput microfluidic microarray platform, we profiled cellular miRNA expression in human epithelial A549 cells infected with S- and A-OIVs at multiple time points during the viral life cycle, including a global gene expression profiling during S-OIV infection. We performed quantitative reverse transcription-PCR (qRT-PCR) to validate the miRNA chip results. We used target prediction and pathway enrichment analyses to identify key cellular pathways associated with the differentially expressed miRNAs and inversely correlated mRNAs during pandemic S-OIV H1N1 and highly pathogenic A-OIV H7N7 infection. Our identification of specific and dynamic molecular phenotypic changes (microRNAome) triggered by S- and A-OIV infection in human cells provides robust experimental evidence demonstrating a series of strain-specific host molecular responses involving different combinatorial contributions of multiple cellular miRNAs. Overall, our results demonstrate a series of complex temporal and strain-specific host microRNA molecular signatures associated with swine-origin H1N1 and avian-origin H7N7 infA infection, and they also identify novel potential secretory miRNA biomarkers associated with pandemic S-OIV and deadly A-OIV-host infections.

MATERIALS AND METHODS

Virus strains and cell lines. All experiments with live influenza virus were performed at the National Center for Foreign Animal Diseases under biosafety level 3 conditions. The influenza A virus strains used in the present study were A/Mexico/InDRE4487/2009 (H1N1) and A/chicken/Germany/R28/2003 (H7N7). A/Mexico/InDRE4487/2009 (H1N1) stocks were propagated on MDCK (Madin-Darby canine kidney) cells, and A/chicken/Germany/R28/2003 (H7N7) virus stocks were propagated on QT-35 cells.

Virus infections. A549 cells were infected with the H1N1 and H7N7 viruses at a multiplicity of infection (MOI) of 0.1. In contrast to highly pathogenic A-OIV H7N7 (23, 58), infection with S-OIV 2009 H1N1 was performed in the presence of 1 μg of TPCK (tolylsulfonyl phenylalanyl chloromethyl ketone)-trypsin (62)/ml. Cell supernatant and RNA were collected at 0, 4, 8, 24, 48, and 72 h postinfection (hpi). The 0-h time point corresponds to samples collected immediately after the 1-h virus incubation, with additional time points numbered with regard to the end of viral incubation. Mock-infected A549 cells were propagated for each experiment with samples collected at the 72-h time point. H1N1 virus titration was done by plaque assays on MDCK cells.

RNA isolation. Total RNA was isolated using an miRvana miRNA isolation kit (Ambion) according to the instructions of the supplier. The concentration of RNA was determined by a NanoDrop ND-1000 Spectrophotometer (Thermo).

miRNA expression profiling. Mirna expression profiling was analyzed with a Geniom real-time analyzer (GRTA; Febit GmbH, Heidelberg, Germany) using the Geniom miRNA *Homo sapiens* biochip. Each array contained seven replicates of 904 miRNAs and miRNA star sequences as annotated in the Sanger miRBase 14.0 (16–18). With a total of eight arrays per chip, the mock-infected RNA was run in duplicate (arrays 1 and 2) with the subsequent time points loaded in order (0 to 72) into arrays 3 to 8. Sample labeling with biotin was carried out by microfluid-based enzymatic on-chip labeling of miRNAs (61). In brief, after hybridization of the miRNA with the Geniom biochip for 14 h at 42°C, the biochip was washed automatically and a program for signal enhancement was processed with the GRTA. The detection pictures were evaluated using the Geniom Wizard software. The raw data values were background-corrected using the median of blank controls. One intensity value was retained for each miRNA by calculating the median for all of the corresponding replicates. Variance stabilizing normalization (26) was applied to normalize the data across different arrays.

mRNA expression profiling. Illumina direct hybridization assays were performed at the Vancouver Prostate Centre Laboratory for Advanced Genome Analysis, Vancouver, British Columbia, Canada. Total RNA quality was assessed with an Agilent 2100 bioanalyzer, and samples with an RNA integrity number (RIN) of ≥8.0 were deemed suitable for microarray analysis. An input of 200 ng of total RNA was used to generate biotin-labeled cRNA according directions for the Illumina TotalPrep RNA amplification kit (Ambion, Inc.). Samples were hybridized on Illumina HumanHT-12 v3 BeadChips according to the Illumina whole-genome gene expression direct hybridization assay guide (document 11286331). BeadChips were imaged and quantified with the Illumina iScan scanner. Illumina GenomeStudio v2010.2 was used for data processing, which included averaging signal intensities for each unique Beadtype. GeneSpring 7.3.1 (Agilent Technologies) was used to median-normalize data to the 25th percentile.

Statistical analysis. Quality assessment for the normalized array data was carried out using the package arrayQualityMetrics (33) in the R statistical software (59). The H1N1 RNA in the uninfected samples in chip 1, and the h 4 samples in chip 2 were found to be degraded during the mRNA profiling; therefore, they were excluded from the statistical analysis. The limma (56) R package was used to identify differentially expressed miRNAs or mRNAs by using a fold change of 2 and a nominal *P* value of 0.05 as the filtering criteria. Hierarchical clustering was performed using average linkage clustering with Euclidean distances, treating samples independently of each other. Volcano plots of the $\log_2$ fold change versus the negative log of nominal *P* values for both H1N1 and H7N7 are provided in Fig. SA3 in the supplemental material.

Identification of miRNA-mRNA binding pairs. miRNA target prediction studies were carried out using the miRanda (version 3.3a) algorithm (9, 30), restricting the search to miRNA 5′ seed pairing and using a score cutoff of 100. In addition, we applied the GenMiR++ algorithm (25) to the H1N1 miRNA and mRNA expression profiles to obtain confidence scores for each miRNA-mRNA prediction (see details in the supplemental material). An interaction network was generated for each time point, where an edge in the network fulfills the following criteria: (i) it connects two nodes that correspond to a differentially expressed miRNA or mRNA at that time point, (ii) the interaction is predicted by miRanda, (iii) the interaction is ranked in the top 50% of the highest GenMiR++ scores, and (iv) the regulation of the nodes linked by the interaction is antagonistic at that time point. The miRNA-mRNA relationships were visualized using Cytoscape (52).

Pathway enrichment analysis. Pathway analysis for predicted mRNA targets from the H1N1 miRNA-mRNA networks was carried out using the InnateDB database (see the supplemental material) (43). A nominal *P* value of 0.01 was used to determine significantly enriched pathways. Pathway enrichment for the H7N7 miRNAs was carried out using the R package miRNApath (7) with pathways from the InnateDB database (see the supplemental material). A *P* value threshold of 0.01 was used to determine

enriched predicted pathways. Pathway ontology was used to cluster pathways into categories (see the supplemental material). For H1N1, the Fisher exact test was used to calculate the overlap between the starting list of mRNAs and the set of mRNA molecules present in a pathway category. For H7N7, the overlap was calculated between predicted miRNA-mRNA interactions for differentially expressed miRNAs and the set of miRNA-mRNA interactions present in an enriched pathway category. This clustering facilitated the simplification and visualization of the change in pathway regulation during the time course of infection.

qRT-PCR. qRT-PCR was carried out on total RNA collected from each time point to determine the amount of viral RNA present. Total RNA was prepared by using the miRvana miRNA isolation kit (Ambion). Each RNA sample was evaluated for viral matrix gene transcript levels in duplicate on the Mx3005p PCR multiplex quantitative PCR instrument (Stratagene) using the Superscript III Platinum One-Step Quantitative RT-PCR system (Invitrogen). Matrix gene forward and reverse primers and probe as described by Spackman et al. were used in the H7N7 experiments (57). A modified version of this assay (62) was used to quantify viral RNA levels in pandemic H1N1 experiments. Three samples from each time point were analyzed in triplicate. The data are represented as the means ± the standard errors of the mean (SEM).

qRT-PCR was used to validate miRNA expression changes using the Agilent Mx3005P real-time PCR system (Agilent) and TaqMan chemistry (Applied Biosystems). Reverse transcription and qPCR primer and probe sets were utilized in a TaqMan miRNA reverse transcription kit and TaqMan miRNA qPCR assays as outlined by the company (Applied Biosystems, catalog no. 4427975 with the following identification numbers: let-7g, 002282; miR-34c-3p, 241009_mat; miR-34b, 002102; miR-766, 001986; miR-449b*, 121215_mat; and miR-30c, 000419). Each miRNA assay was run using at least three independent RNA samples per time point in triplicate. RNU6B was used as an endogenous control. The data are represented as the means ± the SEM. Two-way analysis of variance (ANOVA) and the Bonferroni post test were used to determine the interaction between time and infection, as well as significance of the miRNA at each time point compared to the mock-infected control samples ($P < 0.05$). A one-way ANOVA was used to determine significant differences between time points (e.g., 0 hpi versus 48 hpi).

Microarray data resource. The microarray data was deposited in the Gene Expression Omnibus (GEO) database (www.ncbi.nlm.nih.gov/geo/) under accession number GSE36555.

RESULTS

Cellular miRNAs signatures in response to pandemic S-OIV H1N1 (2009) infection in human epithelial A549 cells. To understand the role of human cellular miRNAs in influenza A virus infection, we profiled the expression of cellular miRNAs following infection with pandemic 2009 H1N1 influenza A virus. A549 cells were infected at an MOI of 0.1 with total RNA samples isolated from infected cells at 0, 4, 8, 24, 48, and 72 hpi. An MOI of 0.1 was chosen to represent a physiologically relevant level of infection and allowed us to monitor cellular miRNA expression in infected cells over a long time course (from 0 to 72 hpi), compared to a higher MOI that would result in a high cytopathic effect in the first 24 h, limiting the number of cells to be profiled for cellular miRNAs. Total RNA from mock-infected samples was extracted at the 72-h time point from each of the three experimental replicates to determine basal miRNA expression. Viral replication efficiency was determined by quantifying the expression level of the viral M gene by qRT-PCR, while infectious virus released was determined by plaque assay (Fig. 1A). New viral RNA was detected at 4 hpi and increased 100-fold by 24 hpi. Infectious virus particles increased by a similar amount between 8 and 24 hpi. The amount of new viral RNA and infectious virus particles remained relatively steady after 24 hpi.

Cellular miRNA expression was determined using the GRTA, which uses an RNA-primed, array-based, Klenow extension assay in conjunction with microfluidic microarray technology (48, 61). Compared to more traditional microarray platforms, the microfluidic platform on the Febit GRTA combines eight customizable arrays on a single chip, with each array containing seven random repeats of the 904 human miRNA and miRNA star sequences, as annotated in the Sanger miRBase 14.0 (16–18, 61). In addition, this assay uses on-chip hybridization and labeling, reducing sample quantity and handling, and it can discriminate between closely related members of the same miRNA family with significantly less cross-hybridization than other traditional microarray platforms (61). By applying this technology to these studies, we were able to run samples from each of the six time points for each experiment in parallel, along with duplicate samples from the mock-infected controls. The number of deregulated miRNAs for each of the indicated time points was determined by a fold change threshold of 2 and a nominal P value cutoff of 0.05 over the mock-infected RNA samples (see Table SA1 and Fig. SA3A in the supplemental material). The expression of each significantly deregulated miRNA across all time points was depicted with a heat map (Fig. 1A). Downregulated miRNAs correspond to 25% of the total differentially expressed miRNAs. At 4 hpi, 9 of 13 miRNAs demonstrated reduced expression, thereby displaying the highest number of downregulated miRNAs compared to any other time point (Fig. 1B). This result contrasts drastically with upregulated miRNAs, which make up 75% of the total differentially expressed miRNAs during pandemic 2009 H1N1 infection across all time points. The number of upregulated miRNAs remains relatively low for the first 24 hpi, where 9% of the total differentially expressed miRNAs are upregulated, before dramatically increasing at 48 and 72 hpi to 91% (Fig. 1C). It is important to note that the subset of significantly downregulated miRNAs at early time points during infection is distinct from the subset of significantly upregulated miRNAs at late time points in infection.

Comparative qRT-PCR analysis was used to further investigate the results from our microarray data. A subset of miRNAs were selected for validation, in particular those deregulated at 72 hpi, based on pathways that were previously reported to be implicated in influenza virus A infection (e.g., cell cycle). Using TaqMan qRT-PCR miRNA arrays, we determined the fold change of multiple miRNAs over the course of infection (Fig. 2A to F). Each graph represents the mean absolute fold change of triplicate experiments for each miRNA at each individual time point compared to mock-infected controls collected at 72 hpi. The significance of interaction between time and infection as well as that of specific miRNAs relative to controls was determined using two-way ANOVA with a Bonferroni post test, while changes between time points were determined using a one-way ANOVA. The miRNA let-7g did not show significant deregulation during H1N1 infection in this experiment, although the qRT-PCR data show a downward trend for this miRNA at early time points (Fig. 2A). Significant upregulation ($P < 0.05$, Bonferroni post test) was observed with miR-34c-3p compared to mock-infected controls at 72 hpi (Fig. 2B). In addition, although neither infection nor time individually contributed to a significant source of variation, the interaction between the two was considered significant ($P = 0.0402$, two-way ANOVA), indicating that both factors are necessary for the differential expression of miR-34c-3p during H1N1

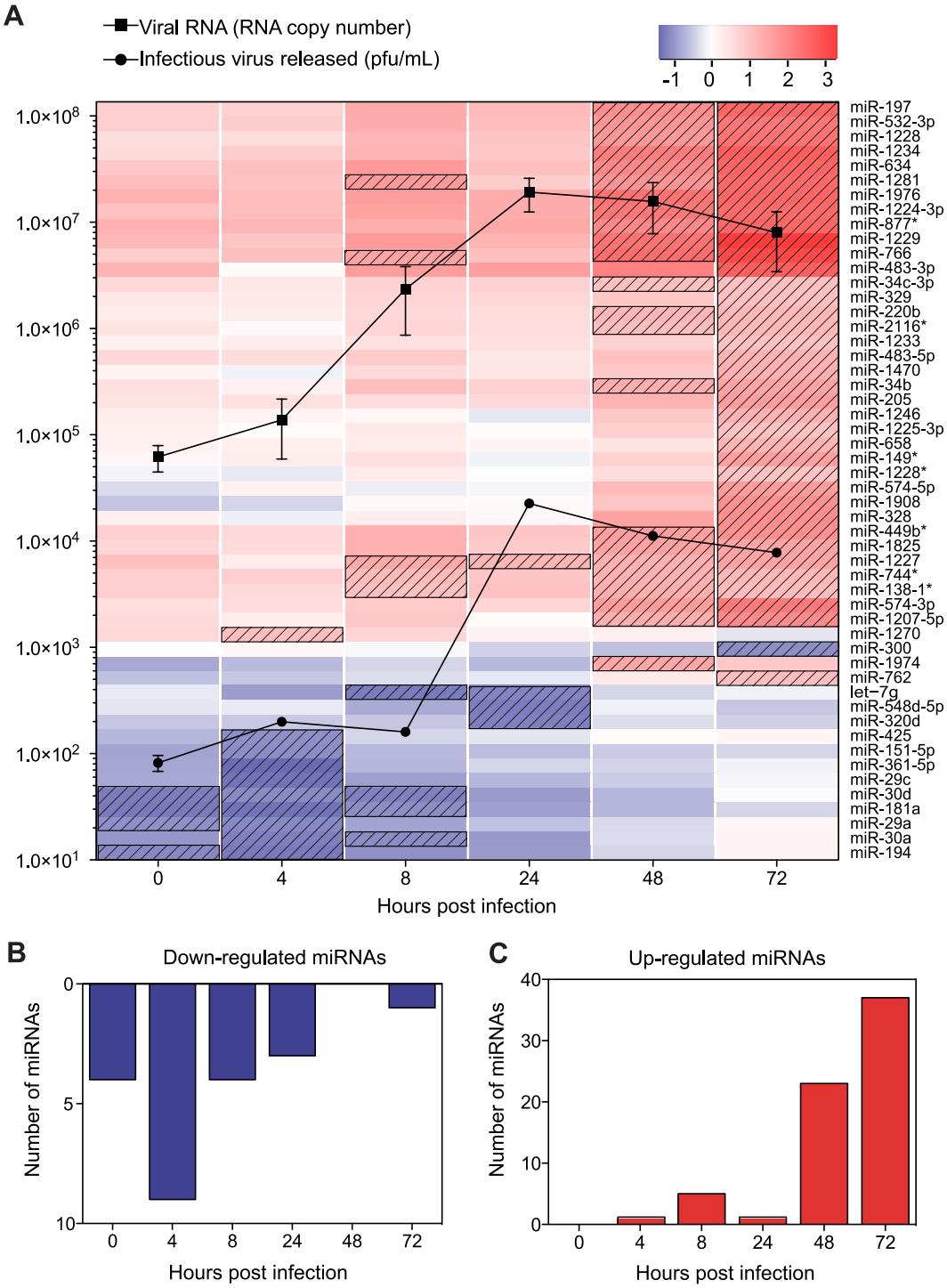

FIG 1 Time point-specific regulation of miRNAs during pandemic 2009 H1N1 influenza A virus infection. (A) Heat map depicting the miRNAs that are differentially expressed at any one time point after infection (total of 52). Colors indicate $\log_2$ ratios of infected versus mock-infected control, according to the specified scale. Red denotes upregulation, while blue indicates downregulation, with hatched cells (▨) highlighting significantly deregulated miRNAs at the corresponding time point. The overlaid curves represent viral replication efficiency as determined by qRT-PCR and infectious virus released as determined by plaque assay. *In vitro*-transcribed RNA of the M gene was used as the standard to determine the RNA copy number. The data are shown as means ± the SEM. (B and C) Numbers of significantly downregulated miRNAs (B) and upregulated miRNAs (C) during the course of infection with pandemic 2009 H1N1 infA. Significance was determined by using a fold change threshold of at least 2 and a nominal *P* value cutoff of 0.05. The *x* axis represents the hours postinfection (0, 4, 8, 24, 48, and 72 hpi).

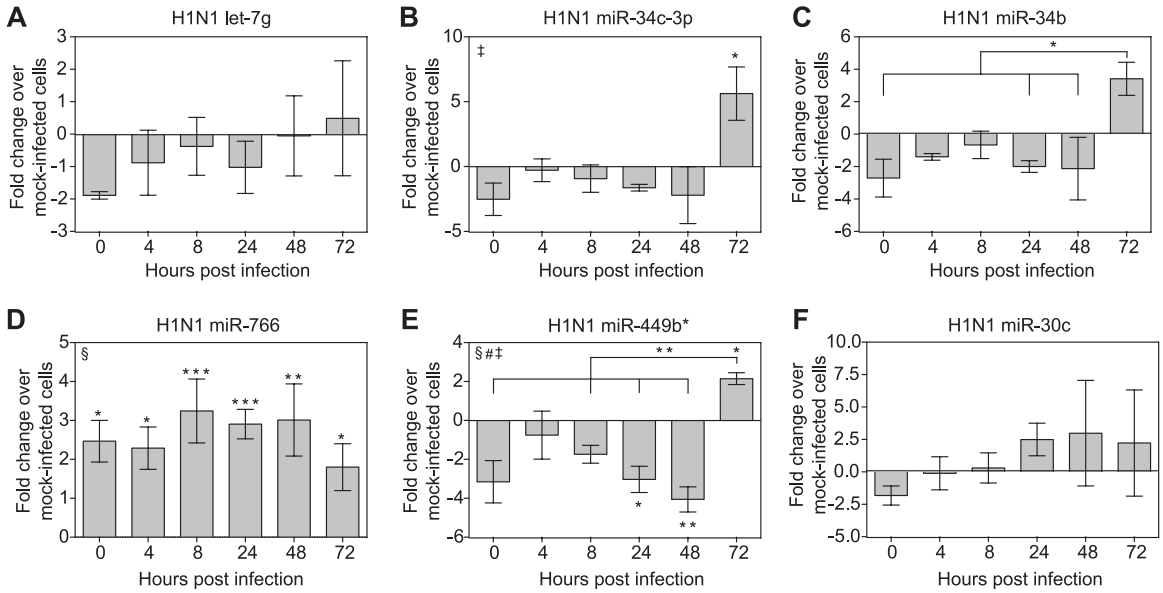

FIG 2 qRT-PCR analysis of miRNA expression during pandemic 2009 H1N1 influenza A virus infection. The results of qRT-PCR analyses of let-7g (A), miR-34c-3p (B), miR-34b (C), miR-766 (D), miR-449b* (E), and miR-30c (F) at six time points after infection are presented. Each graph represents the mean absolute fold change of triplicate experiments for each miRNA at six individual time point compared to mock-infected controls collected at 72 hpi. All qRT-PCR data are represented as means ± the SEM. Significance is based on one-way and two-way ANOVA and Bonferroni post test analyses (*, $P < 0.05$; **, $P < 0.01$; ***, $P < 0.001$). The notation in the top left corners of the panels corresponds to the significance determined by two-way ANOVA for infection (§), time (#), and interaction between time and infection (‡).

infection. The expression level of miR-34b at 72 hpi was significantly different compared to 0, 24, and 48 hpi by one-way ANOVA; however, there was no significance attributed to either time or infection by two-way ANOVA analysis (Fig. 2C). Consistent upregulation across all six time points was observed with miR-766, and two-way ANOVA confirmed that infection is the main factor in miR-766 deregulation ($P < 0.001$), accounting for ca. 56% of the total variance (Fig. 2D). The expression of miR-449b* changes dramatically along the course of infection (Fig. 2E). At early time points (0 to 48 hpi), the levels of miR-449b* are lower than in mock-infected cells, with the levels at 24 and 48 hpi showing significant downregulation. A significant shift occurs between 48 and 72 hpi, where miR-449b* becomes more abundant at 72 hpi than in uninfected cells. The interaction between infection and time was considered significant by two-way ANOVA ($P = 0.0001$), while infection and time independently also affect the result significantly ($P = 0.0003$ and 0.0001, respectively). This is in contrast to the microarray data that showed a significant upregulation of miR-449b* at 48 and 72 hpi. Differences in the platforms used for analysis can lead to differences in fold changes (4), which may explain the loss of significance at certain time points in the qRT-PCR data compared to microarray data. It has also been shown that genes can appear to be regulated in opposite directions using different platforms (4, 11). The methods may also disagree when the miRNAs have lower expression level, due to the greater sensitivity of the qRT-PCR assay (5). In addition, different detection techniques will show variation due to mixed populations of miRNAs that can exist in the cell (61). In light of all this, we consider the microarray results only to acquire a global picture of the trends of miRNA deregulation and affected pathways and use the qRT-PCR validations when focusing on the regulation of specific miRNAs. The validation of miR-30c by RT-PCR did not result in significance of expression, and this was also true with the array data (Fig. 2F).

Dynamic changes in the host cell miRNA-mRNA interactome induced by the 2009 pandemic influenza (H1N1) virus. To study the modulation in gene expression that may be associated with specific miRNAs, we performed global transcriptome analysis in A549 cells during pandemic 2009 H1N1 influenza virus A infection with similar parameters as for the miRNA experiment. The number and trend of deregulated genes during early time points postinfection reflected a similar pattern as that observed for the miRNAs (range, 0.12 to 0.37% [lowest at 24 hpi]). The number of upregulated genes starts to increase after 24 hpi and peaks at 72 hpi (1.26% of the total genes tested). The biological relevance of the host genes expressed during 2009 pandemic H1N1 infection was determined using gene ontology and pathway analysis from InnateDB (43; data not shown). Since miRNAs function to suppress gene expression either by inhibiting translation or by degrading mRNA, we examined those miRNAs that satisfied the following criteria: (i) they are differentially expressed in the H1N1 miRNA microarray expression profile, (ii) they are predicted to target differentially expressed mRNAs from the gene expression profile, (iii) the miRNA-mRNA prediction is found in the top 50% highest scores from the GenMiR++ algorithm, and (iv) the direction of their regulation is antagonistic to the predicted targets. The collection of differentially expressed mRNA and miRNA sequences was analyzed using the miRanda algorithm (version 3.3a) to determine potential miRNA-mRNA target interactions. The miRanda algorithm identifies strong seed region base pairing between the miRNA and mRNA 3′UTRs (60). High scoring targets are then filtered by predicted heteroduplex free energy (ΔG) and conservation of the predicted binding site. The miRanda pre-

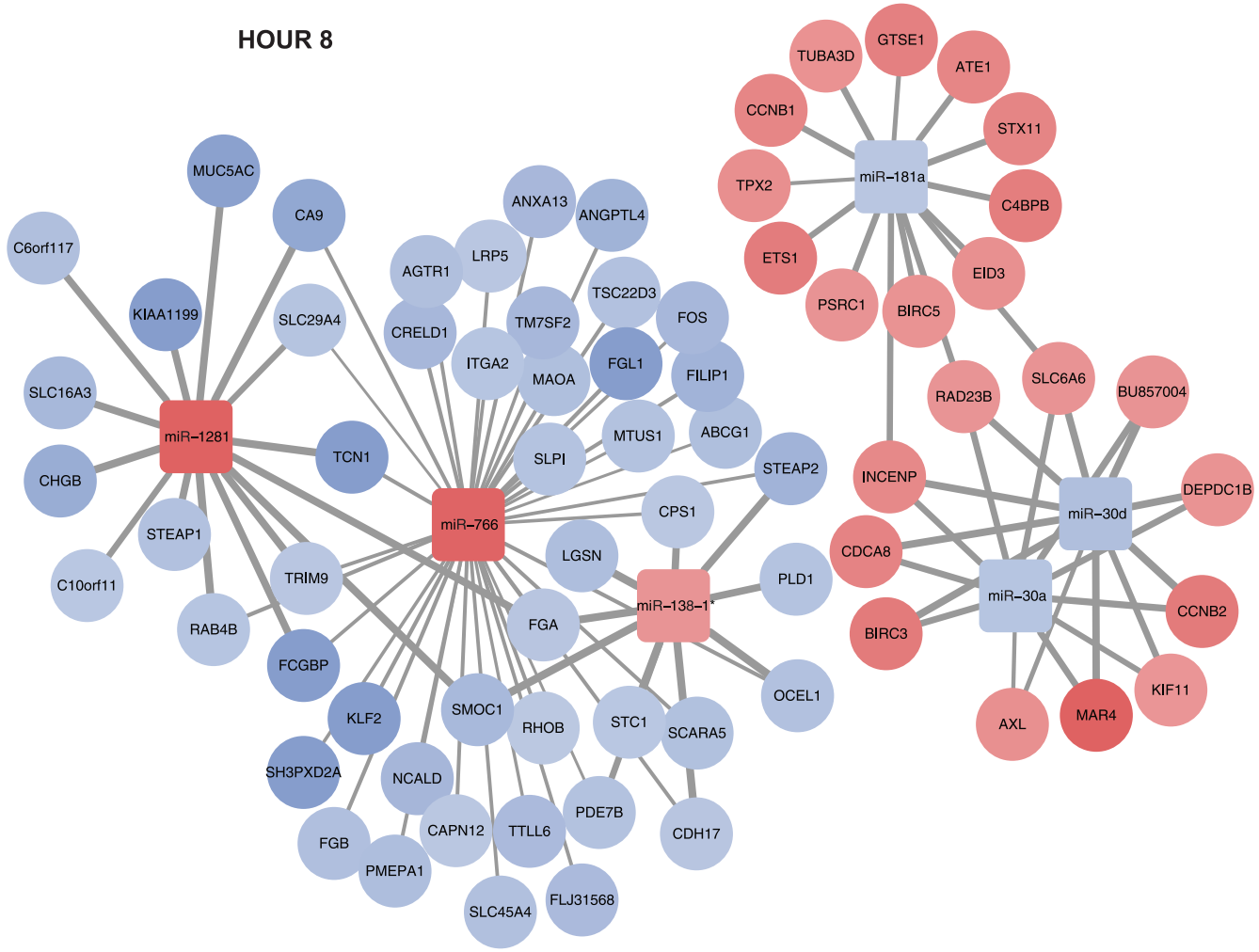

FIG 3 Complexity of the miRNA-mRNA interactome network at 8 h after infection with pandemic 2009 H1N1 influenza A virus. Temporal and global molecular phenotypic changes triggered by infection in human A549 cells at 8 hpi. The network displays predicted interactions between deregulated miRNAs and deregulated mRNAs from two microarray experiments and were generated using a fold-change cutoff ± 2, $P < 0.05$, miRanda target prediction, GenMiR++ scoring, and negative-correlation filtering. Red indicates upregulated miRNAs and mRNAs, while blue indicates downregulation. miRNAs are noted by squares, while mRNA nodes are depicted as circles. The thickness of the edges corresponds to the GenMiR++ scores.

dictions were further filtered according to confidence scores obtained from GenMiR++ (25; see also the supplemental material).

The predicted interactions between differentially expressed miRNAs and predicted target mRNAs from our microarray experiments were visualized as networks in order to depict the complex relationship associated with miRNA gene regulation, which increases dramatically from 0 to 72 hpi (Fig. 3; see also Fig. SA1A to D in the supplemental material). The number of upregulated miRNAs in each network increases as the infection progresses, from 0 miRNAs at 0 and 4 hpi (see Fig. SA1A and B in the supplemental material) and 3 miRNAs at 8 hpi (Fig. 3) to 20 miRNAs at 48 hpi (see Fig. SA1C in the supplemental material) and 28 miRNAs at 72 hpi (see Fig. SA1D in the supplemental material), which correlates with targeted mRNAs being downregulated at 48 and 72 hpi. In contrast, the number of downregulated miRNAs peaks at 4 hpi, with 48 and 72 hpi showing almost no downregulation (0 and 1 miRNAs, respectively [see Fig. SA1C and D in the supplemental material]). The 8-hpi network (Fig. 3) shows a number of deregulated miRNAs and their predicted targets, including miR-766, that is consistently upregulated throughout infection with H1N1 (Fig. 2D). A dramatic drop in differentially expressed miRNAs at 24 hpi resulted in no significant miRNA-mRNA interactions. By 72 hpi, most miRNAs are upregulated, correlating with downregulated targets such as Rbl1, Cdt1, E2f7, Mcm4, and Mcm7. The predicted target mRNAs from the interaction networks were explored further using InnateDB to identify pathways that are enriched in these networks and that may be relevant to influenza virus A infection (Fig. 4; see also Tables SA2 and SA3 in the supplemental material). The number of pathways and mRNAs associated with each miRNA at different time points was influenced by our prediction analysis and data published to date. By 72 hpi, a majority of the pathways were downregulated and were represented by genes associated with cell cycle, including but not limited to the E2F transcription factor network, CDK regulation of DNA replication, and G_1/S transition (Fig. 4 and see Table SA2 in the supplemental material). Replication and repair, as well as chromosome maintenance and signaling pathways, were also downregulated at 72 hpi.

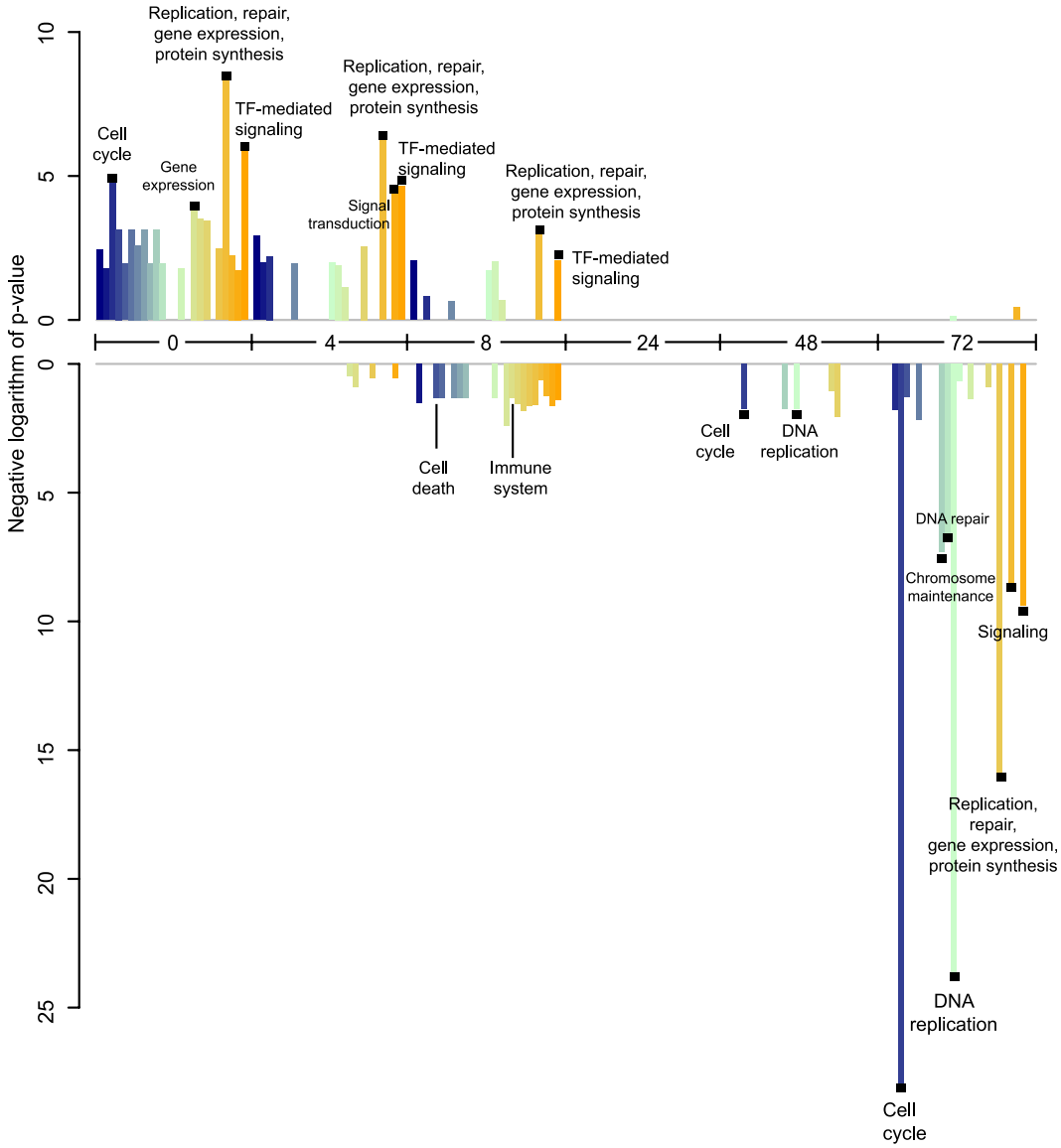

FIG 4 Canonical pathways implicated in infection with pandemic 2009 H1N1 influenza A virus from dual expression studies. Pathways affected by deregulated mRNAs involved in the miRNA-mRNA interactions (targeted mRNAs). The pathways were clustered according to pathway ontology into categories. Bars above the zero line depict pathways where the majority of the implicated mRNAs were upregulated in the expression analysis, while bars below the zero line show pathways represented by downregulated mRNAs. The most abundant pathway categories are labeled. The *y* axis indicates the significance of overlap (in the form of negative log of *P* values) between the input mRNA list and the set of mRNA molecules in a particular pathway category. The *x* axis represents hours postinfection (0, 4, 8, 24, 48, and 72 hpi).

Cellular miRNA signatures in response to highly pathogenic A-OIV H7N7 (2003) infection in human epithelial A549 cells. Since we sought to understand the impact of viruses with various pathogenicity on host cells, we continued our study by investigating the dynamic modulation of miRNAs during infection with a highly pathogenic avian H7N7 strain (Fig. 5; see also Table SA4 in the supplemental material). A549 cells were infected at an MOI of 0.1, and total RNA samples from infected cells were isolated at the indicated time points. Viral replication efficiency was determined by quantifying the expression level of the viral M gene by qRT-PCR with new viral RNA detected by 8 hpi (Fig. 5A). The number of deregulated miRNAs was determined by using the same parameters as for H1N1 (see the volcano plots in Fig. SA3B in the supplemental material). As with our results for the H1N1 experiment, we observed a similar trend in miRNA expression with a downregulation of miRNA expression at early time points (0 to 24 hpi) and upregulation of miRNAs at later time points (48 to 72 hpi). In contrast to the H1N1 study, the number of differentially expressed miRNAs was considerably higher during H7N7 infection: a total of 121 miRNAs showed significant deregulation at some point postinfection compared to 52 miRNAs for pandemic 2009 H1N1 (Fig. 5A). The percentage of miRNAs that are downregulated during infection with H7N7 reaches 54%, being distributed more densely (70% of total downregulated miRNAs) at the early stages of infection (0 to 24 hpi) (Fig. 5B). Similar to H1N1, a stark transition is observed at 48 and 72 hpi, where the percentage of up-

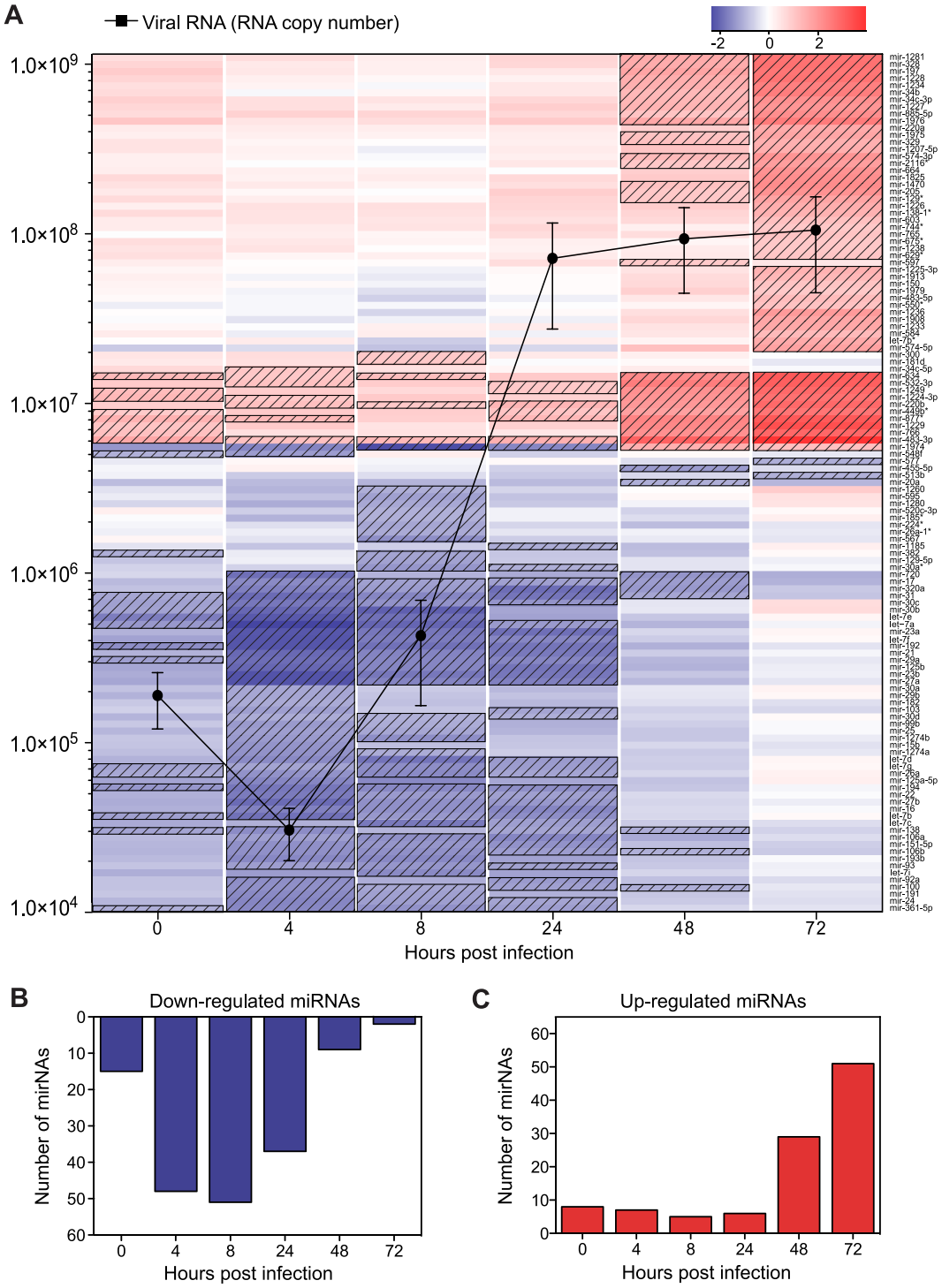

FIG 5 Time-specific regulation of miRNAs during infection with highly pathogenic H7N7 avian influenza A virus. (A) Heat map depicting the miRNAs that are differentially expressed at any one time point after infection (total of 121). Colors indicate the $\log_2$ ratios of infected versus mock-infected control, according to the specified scale. Red denotes upregulation, while blue indicates downregulation, with hatched (▨) cells highlighting significantly deregulated miRNAs at the specified time point. The overlaid curve represents the viral replication efficiency as determined by qRT-PCR. *In vitro*-transcribed RNA of the M gene was used as the standard to determine the RNA copy number. The data are shown as means ± the SEM. (B and C) Numbers of significantly downregulated miRNAs (B) and upregulated miRNAs (C) during the course of infection with highly pathogenic H7N7 avian influenza A virus. Significance was determined by using a fold change threshold of at least 2 and a nominal *P* value cutoff of 0.05.

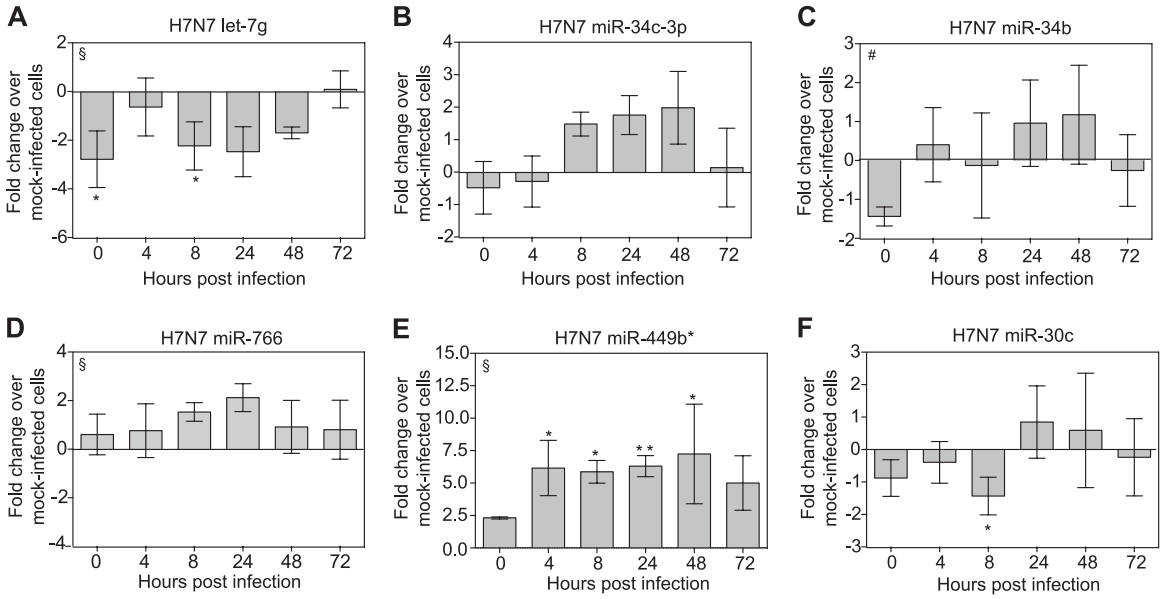

FIG 6 Validation of miRNAs expressed during highly pathogenic H7N7 avian influenza A virus infection using comparative qRT-PCR. The results of qRT-PCR analyses of let-7g (A), miR-34c-3p (B), miR-34b (C),) miR-766 (D), miR-449b* (E), and miR-30c (F) for each time point are presented. Each graph represents the mean absolute fold change of triplicate experiments for each miRNA at six individual time points compared to mock-infected controls collected at 72 hpi. All qRT-PCR data are represented as means ± the SEM. Significance is based on one- and two-way ANOVA and Bonferroni post test analyses (*, $P < 0.05$; **, $P < 0.01$; ***, $P < 0.001$). The notation in the top left corners of the panels corresponds to the significance determined by two-way ANOVA for infection (§), time (#), and interaction between time and infection (‡).

regulated miRNAs relative to the total number of upregulated miRNAs is higher than at earlier time points (81%) (Fig. 5C).

Comparative qRT-PCR analysis of deregulated miRNAs (up- and downregulated) during highly pathogenic H7N7 infection was used to further investigate the validity of the microarray results in the same manner as for the H1N1 study (Fig. 6). The miRNA let-7g was found to be significantly downregulated at 0 and 8 hpi, and infection was considered to significantly affect the miRNA deregulation ($P < 0.0001$, two-way ANOVA) (Fig. 6A). There was no significant upregulation of miR-34c-3p expression at any time point by two-way ANOVA and Bonferroni post test ($P > 0.05$, Fig. 6B). Although the individual time points for miR-34b and miR-766 did not show differential expression relative to control by Bonferroni post tests, the effect of time or infection on miRNA expression for miR-34b and miR-766, respectively, was considered significant by two-way ANOVA ($P = 0.0344$ and 0.0046, respectively) (Fig. 6C and D). In addition, consistent upregulation of miR-449b* across four time points (4, 8, 24, and 48 hpi) was observed (Fig. 6E) and a significant P value (<0.0001, two-way ANOVA) confirmed that infection accounts for almost 59% of the total variance observed. While not significant by two-way ANOVA, the downregulation of miR-30c was considered significant at 8 hpi according to Bonferroni post tests (Fig. 6F).

Significantly expressed miRNAs during infection with H7N7 were subjected to target prediction and pathway enrichment analyses using miRanda, the InnateDB pathway database, and the miRNApath R package (7). A P value cutoff 0.01 was used to determine significantly enriched predicted miRNA target pathways (Fig. 7; see also Tables SA5 and SA6 in the supplemental material). Transmembrane transport of small molecules, metabolism of proteins and carbohydrates, signaling by G protein-coupled receptor, infectious disease-related pathways, and cell cycle dominate the spectrum of enriched pathways at the early stages of infection with H7N7. The number of enriched pathways is reduced at 24 hpi when signal transduction and cell proliferation pathways are active, while metabolic pathways and chromosome maintenance are observed at 48 hpi.

Common and distinct host cell miRNA signatures associated with pandemic S-OIV H1N1 and highly pathogenic A-OIV H7N7 infections. The comparison of differentially expressed miRNAs from each microarray experiment identified miRNAs whose expression profiles differed between H1N1 infection and H7N7 infection. A total of 40 miRNAs were commonly differentially expressed between both influenza virus A strains, with 33 being upregulated (82.5%, Fig. 8A; see also Fig. SA2A in the supplemental material) and 7 being downregulated between both viruses (Fig. 8B; see also Fig. SA2B in the supplemental material). Interestingly, 23 miRNAs were identified as being significantly upregulated only during H7N7 infection by microarray analysis, compared to only six uniquely upregulated miRNAs associated with H1N1 (Fig. 8A). Included in the list of upregulated common miRNAs is miR-449b*, which we validated as being significantly upregulated by qRT-PCR for both H1N1 and H7N7 (Fig. 2E and Fig. 6E). In addition, miR-449b* had a significantly higher fold change during H7N7 infection compared to that during H1N1 infection as determined by qRT-PCR (Table 1).

In contrast to the upregulated miRNAs, very few common downregulated miRNAs were identified. A total of 72 miRNAs were found to be downregulated during infection with both strains of influenza A virus, of which 59 were significantly downregulated only during H7N7 infection by microarray analysis (Fig. 8B). Only seven downregulated miRNAs (17.5%) were found to be common between the two viruses. At 4 hpi, a total of six miRNAs were shared between the two viruses, the

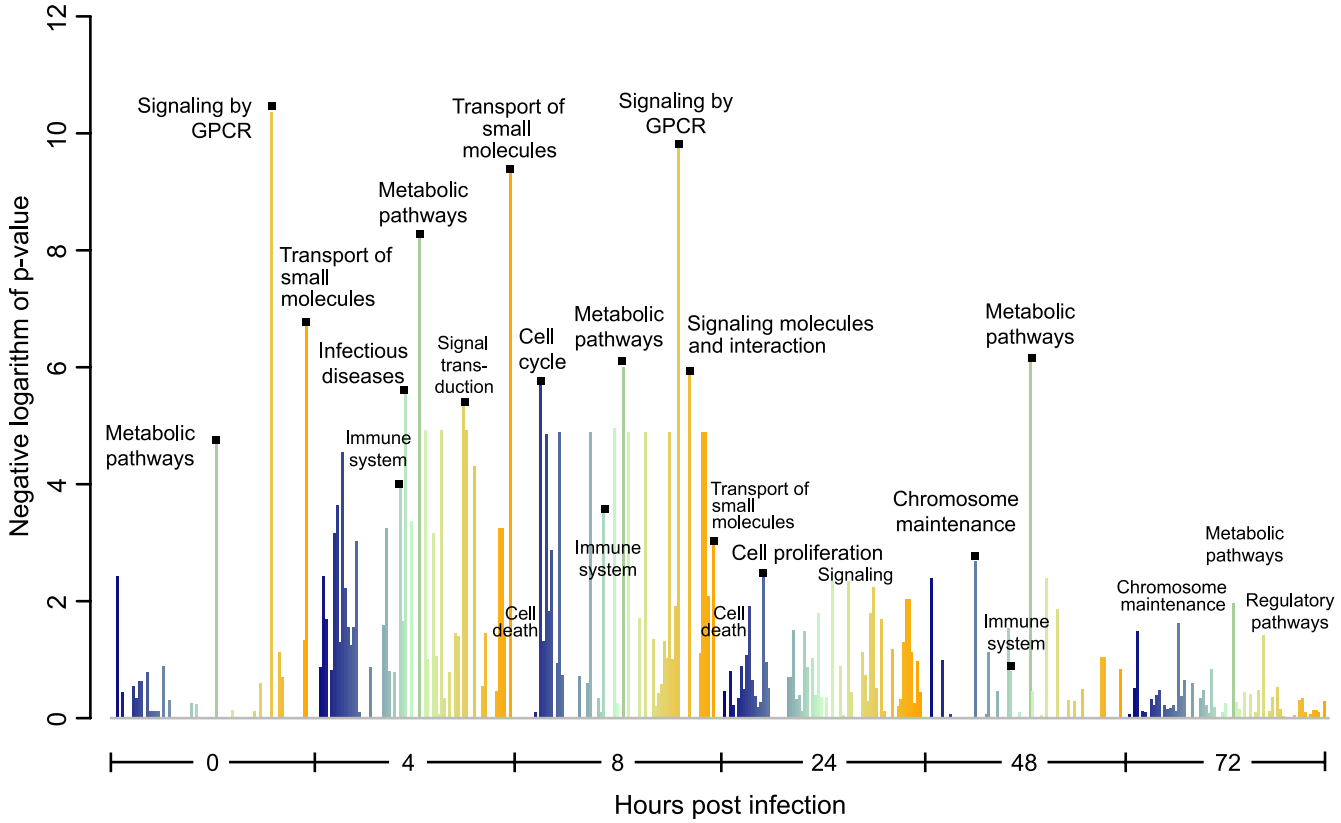

FIG 7 Pathways predicted to be affected by the deregulated miRNAs during highly pathogenic H7N7 avian influenza A virus infection. Significantly expressed miRNAs during infection with highly pathogenic H7N7 avian influenza A virus were subjected to target prediction and pathway enrichment analyses. All pathways were obtained from the InnateDB database and analysis performed using miRNApath package in R. A *P* value cutoff of 0.01 was used to determine significantly enriched pathways. Pathways were clustered into categories using pathway ontology from the relevant sources, and the most abundant pathway categories are labeled. The *y* axis indicates the significance of overlap (in the form of negative log of *P* values) between predicted miRNA-mRNA pairs (for deregulated miRNAs) and the set of miRNA-mRNA pairs found in a particular pathway category.

highest for any time point (see Fig. SA2B in the supplemental material). However, 42 downregulated miRNAs were unique to H7N7 at the same time point, and this number increased to 49 miRNAs at 8 hpi (see Fig. SA2B in the supplemental material). Of the common miRNAs, we previously demonstrated that let-7g was significantly downregulated during H7N7 infection (Fig. 6A). This miRNA also showed a trend of downregulation across all early time points during H1N1 infection but was not found to be significant by qRT-PCR (Fig. 2A).

qRT-PCR validation demonstrated that miR-30c was significantly downregulated during H7N7 infection at 8 hpi (Fig. 6F). We confirmed that expression of miR-30c was not significantly up- or downregulated at any of the six time points during H1N1 infection (Fig. 2F). We have also shown that both miR-34b and miR-34c-3p are not significantly deregulated during H7N7 infection. This is in contrast to H1N1 where miR-34c-3p is almost 5-fold upregulated at 72 hpi and miR-34b expression is upregulated at 72 hpi, a significant difference from its expression at 0, 24, and 48 hpi. All together, we have identified three miRNAs (miR-34b, miR-34c-3p, and miR-449b*) that show significantly different expression profiles between H1N1 and H7N7 infection (Table 1). Taken together, our data demonstrate that a number of miRNAs are expressed in a strain-specific manner during influenza virus A infection.

Exosome-associated miRNAs are deregulated during S- and A-OIV infections. To date, 413 unique miRNAs and 2068 proteins have been found in human exosomes (Exocarta v3.1) (44, 45, 53, 54). Our bioinformatics analysis of the differentially expressed cellular miRNAs during infA infection reveals that 47% (6/11) of the miRNAs deregulated with pandemic H1N1 have also been reported in human exosomes as opposed to 55% (48/81) in the case of highly pathogenic H7N7 (Fig. 9). Interestingly, the majority of these exosome-associated miRNAs were downregulated in our studies. Up to 45% of the common miRNAs differentially expressed during H1N1 and H7N7 viral infections are also found in secretory exosomes (Fig. 9). When we compared the total number of differentially expressed miRNAs for each infA with the total number of miRNAs reported in the Exocarta database ($n = 413$), we found an 8-fold increase in the H7N7-specific exosomal miRNAs (48/413 [11.6%]) compared to the H1N1-specific H1N1 miRNAs (6/413 [1.45%]). This interesting finding may underline an important differential contribution of these newly identified exosomal miRNAs in the S- and A-OIV life cycle and pathogenesis.

DISCUSSION

The results of our study provide the first experimental evidence demonstrating the complex temporal and strain-specific regula-

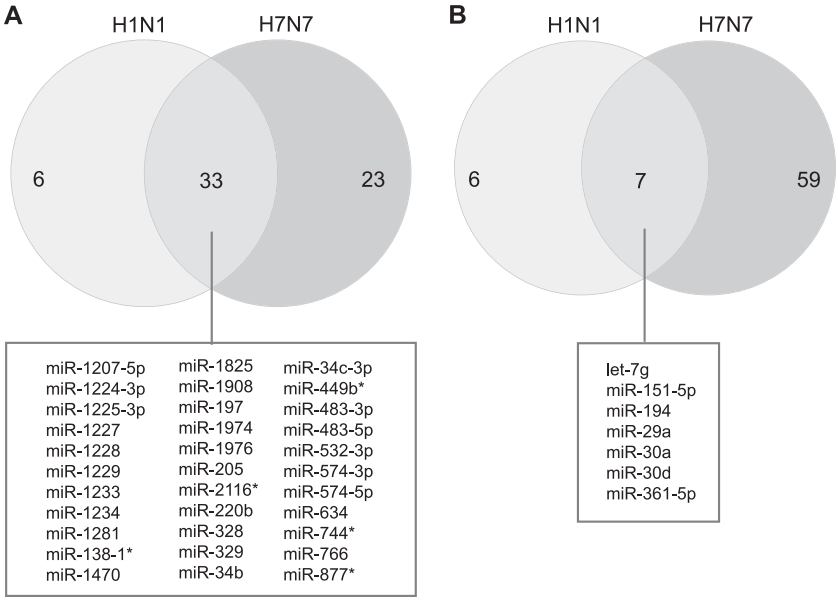

FIG 8 Comparison of miRNAs expressed during infection with pandemic 2009 H1N1 and highly pathogenic H7N7 avian influenza A viruses. (A) Venn diagram of significant upregulated miRNAs during H1N1 and H7N7 infection relative to untreated control. Of the 62 miRNAs found to be upregulated during infection with both strains of influenza A virus, 23 miRNAs were identified by microarray analysis as being significantly upregulated only during H7N7 infection. The diagram displays the names of the 33 common miRNAs that were significantly upregulated during the course of infection. (B) Venn diagram of significant downregulated miRNAs during H1N1 and H7N7 infection. Of the 72 miRNAs found to be downregulated during infection with both strains, 59 were identified by microarray analysis as being significantly downregulated only during H7N7 infection. The list shows the seven common miRNAs that were significantly downregulated during the course of infection.

TABLE 1 Comparison of qRT-PCR-validated miRNAs between pandemic 2009 H1N1 and highly pathogenic H7N7 avian influenza A virus infection

MicroRNA	Time point (h)	Mean fold change[a]		Mean difference ± SEM	P^b
		H1N1	H7N7		
let-7g	0	–1.8865	–2.7819	0.8955 ± 1.705	0.6157
	8	–0.3756	–2.2326	1.857 ± 1.437	0.2146
miR-34b	48	–2.1247	0.9588	–3.302 ± 2.251	0.1859
	72	3.4129	1.1775	3.669 ± 1.402	**0.0308**
miR-34c-3p	24	–1.6254	1.7561	–3.382 ± 0.6535	**0.0066**
	72	5.6259	0.1398	5.486 ± 3.083	0.1055
miR-449b*	0	–3.1523	2.3164	–5.469 ± 1.089	**0.0074**
	4	–0.7556	6.1617	–6.917 ± 2.463	**0.0484**
	8	–1.7386	5.8693	–7.608 ± 0.9904	**0.0015**
	24	–3.0287	6.3018	–9.331 ± 1.057	**0.0009**
	48	–4.0572	7.2433	–11.30 ± 3.892	**0.0440**
	72	2.1478	5.0073	–2.859 ± 1.267	0.0504
miR-30c	8	0.3046	–1.4319	1.736 ± 1.167	0.1650
miR-766	0	2.4670	0.6039	1.864 ± 0.9390	0.0944
	4	2.2880	0.7648	1.523 ± 1.085	0.2100
	8	3.2420	1.5320	1.710 ± 1.130	0.1808
	24	2.9060	2.1260	0.7802 ± 0.6559	0.2792
	48	3.0120	0.9178	2.094 ± 1.471	0.2045
	72	1.8000	0.8046	0.9956 ± 1.221	0.4358

[a] The mean fold changes from specific miRNAs found to be significantly up- or downregulated at indicated time points by qRT-PCR were compared to the corresponding time point associated with either pandemic 2009 H1N1 or highly pathogenic H7N7 avian influenza A viruses.
[b] A two-tailed *t* test determined significance with a *P* value cutoff of 0.05. Significant values are indicated in boldface.

tion of the host microRNAome by S- and A-OIV infections in human cells. The integration of array chip technology, qRT-PCR, and target prediction and pathway enrichment analyses has allowed us to perform a robust comparative genomics and bioinformatics study to reveal the host miRNA molecular signatures associated with S- and A-OIV infections. Our results also reveal the common and specific cellular pathways associated with the differentially expressed host miRNAs during the H1N1 and H7N7 infA life cycles. We identified a unique series of temporal and strain-specific host molecular responses involving different combinatorial contributions of multiple cellular miRNAs, providing, for the first time, key molecular insights into unique cellular miRNA-mRNA interactome networks dynamically and temporally regulated by S- and A-OIV infections.

Temporal host miRNA molecular signatures associated with pandemic S-OIV H1N1 and highly pathogenic A-OIV H7N7 infection. Using a microfluidic microarray approach, we profiled the expression of all human miRNAs (miRBase version 14) across multiple time points after infection with pandemic 2009 S-OIV H1N1 and highly pathogenic A-OIV H7N7 influenza A viruses (Fig. 1A and 5A). One of the most striking observations from the present study is the temporal regulation of host cell miRNAs during the course of infection. During the early stages of infection, from 0 to 24 hpi, the majority of differentially expressed miRNAs were downregulated (Fig. 1B and 5B). The downregulation of miRNAs was more pronounced with the highly pathogenic H7N7 strain than with the low-pathogenic H1N1 strain. The upregulated pathways at 0 to 24 hpi with H1N1 include cell cycle, replication, repair, gene expression, protein synthesis, and signaling pathways (Fig. 4; see also Tables SA2 and SA3 in the supplemental material). Furthermore, the majority of downregulated pathways

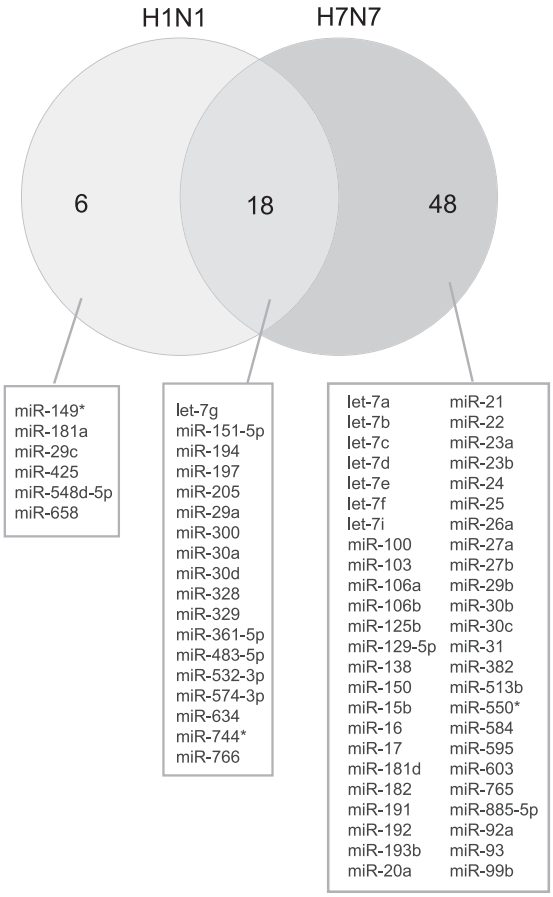

FIG 9 Differentially expressed exosomal miRNAs during infection with pandemic 2009 H1N1 and highly pathogenic H7N7 avian influenza A viruses. Strain-specific regulation of exosome-associated miRNAs is predicted for 6 and 48 miRNAs, respectively, during H1N1 and H7N7 infection. Of the 72 deregulated exosomal miRNAs, 18 are common to H1N1 and H7N7 viral infection. The diagram displays the list of the specific and common exosomal miRNAs (Exocarta v3.1) that were significantly deregulated during the course of infA infection.

at early time points (0 to 24 hpi) with H1N1 infection are associated with immune system and homeostasis (Fig. 4; see also Tables SA2 and SA3 in the supplemental material). In the case of H7N7, more than half of the differentially expressed miRNAs was downregulated, mostly at early time points (0 to 24 hpi) postinfection (Fig. 5B and see Table SA4 in the supplemental material). Among these are miR-24, the let-7 family, the miR-30 family, the miR-29 family, miR-125b, miR-192, miR-191, and miR-99b, which have been associated with a variety of important pathways, including TGFβ signaling, stress response, cell proliferation, apoptosis, oncogene activation, and the cell cycle and inflammatory response pathways in the lung due to exposure to toxins, namely, lipopolysaccharide, formaldehyde, or cigarette smoke (28, 50, 51). For example, the exosome-associated miR-24 is uniquely downregulated at 4, 8, and 24 hpi with H7N7 (Fig. 5 and see Table SA4 in the supplemental material). With the recent demonstration that miR-24 targets the cellular proprotein convertase furin (41), an essential enzyme involved in the proteolytic activation of highly pathogenic H7 and H5 hemagglutinin precursor molecules (HA0) (23, 58), our results suggest that H7N7-mediated miR-24 downregulation would allow host cells to rapidly biosynthesize furin molecules, which are required to cleave HA0 molecules in the secretory pathway. It is tempting to suggest that the proposed virus-specific miRNA-dependent regulatory mechanism of furin activity could play an important role in the distinct pathogenesis associated with S-OIV and highly pathogenic A-OIV infections. Alternately, we observed an H7N7-specific downregulation of miR-30 family members along with an enrichment of cell death pathways at 4, 8, and 24 hpi (Fig. 6 and 7; see also Table SA5 in the supplemental material). Interestingly, downregulation of the miR-30 family members, which includes miR-30c, was also observed in macaques infected with highly pathogenic avian H5N1 influenza A virus, and it may be involved in regulating genes associated with cell death (37), since highly pathogenic infA are known to cause enhanced inflammatory responses, resulting in hypercytokinemia and severe lung damage.

At later stages of infection (48 to 72 hpi), the majority of miRNAs were upregulated with both infA strains. For H1N1, this correlated with a strong downregulation of enriched cellular pathways associated with cell cycle, replication and repair, signaling, and chromosome maintenance (Fig. 4; see also Table SA3 in the supplemental material). Comparatively, at 48 to 72 hpi with H7N7, we observed pathways associated with metabolism, chromosome maintenance, biological oxidation, and regulatory pathways (Fig. 7 and see Table SA6 in the supplemental material). Our qRT-PCR data identified miR-449b* as being significantly upregulated at 72 hpi during H1N1 infection and at 4 to 48 hpi during H7N7 infection (Fig. 2E and 6E). It is known that the downregulation of mRNAs targeted by miR-449a/b can result in cell cycle arrest at G_1 and the promotion of apoptosis (39, 63). In contrast to the temporal modulation of miR-449b*, miR-766 was significantly upregulated at all time points during H1N1 infection (Fig. 2D). The direct targets of miR-766 have not been identified, but its predicted targets are involved in pathways associated with cell survival after chemotherapy and aging (27, 64). The deregulation of these miRNAs, along with others, indicate that the downregulation of cell cycle-related pathways is an important feature of infA infection.

Strain-specific host miRNA molecular signatures associated with pandemic S-OIV H1N1 and highly pathogenic A-OIV H7N7 infection. The expression profiles resulting from our studies provide unique insights into the miRNAs that are significantly differentially expressed during viral infection with two important strains of influenza A virus (pandemic H1N1 and highly pathogenic H7N7) that are associated with distinct pathogenesis. Strain-specific patterns of miRNA expression were first observed when examining the global expression signatures, where the number of differentially expressed miRNAs in the A-OIV H7N7-infected cells was double that seen during S-OIV H1N1 infection (Fig. 8; see also Fig. SA2 in the supplemental material). Of the miRNAs that have common expression between the two viruses, upregulated miRNAs were most represented. In turn, a higher number of miRNAs unique to H7N7 were downregulated, indicating that the avian strain allows the enrichment of a larger number of cellular pathways (observed at early time points in Fig. SA2 in the supplemental material). Three miRNAs (miR-34c-3p, miR-34b, and miR-766) were upregulated during H1N1 infection according to RT-PCR data (Fig. 2B, C, and D), but they showed no significant up- or downregulation during H7N7 infection (Fig. 6B, C, and D). In addition, the expression of let-7g, a member of

the highly conserved let-7 family, and of miR-30c was significantly downregulated only at early time points during H7N7 infection, further establishing a possible role for these and other downregulated miRNAs early during H7N7 infection (Fig. 6A and F). Even miR-449b*, which was significantly upregulated at multiple time points during H7N7 infection, differed compared to the H1N1 expression profile (Fig. 6E and Table 1). The miR-449 and miR-34 families of miRNAs are activated by E2F1 and p53, respectively, in response to DNA damage and are found to target a number of cell cycle-related mRNAs (13, 21, 39, 63, 66). Targets of miR-449a/b include Cdk6 and Cdc25a, while the miR-34 family functions as tumor suppressors by targeting antiapoptotic mRNAs, including Ccne2, Bcl-2, and Cdk6 (21, 39, 63). Regulation of these mRNAs by the miR-449 and miR-34 families causes cell cycle arrest at G_0/G_1 and the induction of apoptosis, both of which have been shown to be important to the infA life cycle (19, 40, 42). Furthermore, profiles of leukocytes from infected patients showed that profound changes in cell cycle regulation were associated with an increase in the severity of disease caused by infA infection (49).

The specific roles of each of these miRNAs during infA infection is still to be determined and is beyond the scope of the present study, but our data do suggest that the strain-specific changes observed here may be another important factor in the distinct pathogenesis associated with S- and A-OIV infections.

Deregulated exosomal miRNAs in infA-infected cells: implications for host responses by intercellular communication and miRNA biomarker discovery. Exosomes are multifunctional bioactive vesicles secreted by both normal and pathological cells, and they can be used for intercellular communication (53, 54). Exosomes contain different types of functional RNA molecules (mRNA and miRNA) and biologically active polypeptides and proteins that can be released into recipient cells (45). Our finding that 47% and 55% of the miRNAs deregulated with pandemic H1N1 and highly pathogenic H7N7, respectively, have also been reported in secretory exosomes is an exciting discovery. Our results support the idea that the specific and dynamic miRNA changes triggered by infA infection in individual cells could be communicated to bystander cells using the host cell exosome pathway. The intercellular communication between infected and uninfected bystander cells would involve newly biosynthesized and strain-specific exosome-associated miRNAs (53). Since secretory exosomes provide a rich source for discovering potential blood-based biomarkers through noninvasive blood tests (12), our findings also raise the possibility of identifying in the very near future circulating miRNA biomarkers to predict clinical progression in infA-associated diseases linked with serious illness, such as the acute respiratory complications previously reported from pandemic H1N1 (2009) infection (46).

Conclusion. As we move into the 21st century, drug-resistant infA are continuously eroding the therapeutic armamentarium, leaving fewer alternative therapeutic agents available (46). More than ever, exploring novel host-directed antiviral targets is important for developing novel global anti-infA strategies that will catalyze the creation of therapeutics with novel mechanisms of action (8, 15, 46). With the recent demonstration by Lanford et al. that anti-miRNA molecules can be successfully used as therapeutic agents against chronic HCV infection in chimpanzees (35), our findings on strain-specific infA regulation of the host-cell microRNAome will certainly catalyze the research on therapeutic silencing of cellular miRNAs as indirect-acting anti-infA agents. Finally, it will be interesting to explore if the specific molecular miRNA signatures identified in our study will translate into the identification of new diagnostic and prognostic secretory miRNA biomarkers in infA-associated diseases. Interestingly, our discovery that a significant number of the host miRNAs identified in our study are putative cargo molecules in secretory exosomes is very exciting and raises the question as to what biological roles these exosome-associated miRNAs may play in infA infection and pathogenesis.

ACKNOWLEDGMENTS

We thank Anne Haegert from the Vancouver Prostate Centre Laboratory for Advanced Genome Analysis for help with the mRNA microarrays, Yohannes Berhane at CFIA for reagents and training, Timm Harder at the Friederich-Loeffler-Institut for providing A/chicken/Germany/R28/03 (H7N7), Andreas Keller from Febit for valuable support in analyzing the microarray data, Chris Fjell for assistance with InnateDB, and Hossein Radfar for assistance with GenMiR++. Westgrid Compute Canada clusters were used for some analyses. We thank Jill Kelly for proofreading of the manuscript.

This study was supported by Canadian Institutes of Health Research team grant TPA-90195 and contract 4500231387 from the Public Health Agency of Canada to F.J. E.-K.L. acknowledges generous support from a National Science Foundation Scholarship.

E.-K.L., F.J., and J.P. conceived and designed the experiments. E.-K.L. and S.D. performed the experiments. E.-K.L., V.S., F.J., S.D., and J.P. analyzed the data. F.J. and J.P. contributed reagents and materials. E.-K.L., V.S., and F.J. wrote the paper.

REFERENCES

1. **Ambros V.** 2004. The functions of animal microRNAs. Nature **431**:350–355.
2. **Bartel DP.** 2004. MicroRNAs: genomics, biogenesis, mechanism, and function. Cell **116**:281–297.
3. **Bartel DP.** 2009. MicroRNAs: target recognition and regulatory functions. Cell **136**:215–233.
4. **Baum M, et al.** 2003. Validation of a novel, fully integrated and flexible microarray benchtop facility for gene expression profiling. Nucleic Acids Res. **31**:e151.
5. **Camarillo C, Swerdel M, Hart RP.** 2011. Comparison of microarray and quantitative real-time PCR methods for measuring MicroRNA levels in MSC cultures. Methods Mol. Biol. **698**:419–429.
6. **Cazalla D, Yario T, Steitz JA.** 2010. Down-regulation of a host microRNA by a herpesvirus saimiri noncoding RNA. Science **328**:1563–1566.
7. **Cogswell JP, et al.** 2008. Identification of miRNA changes in Alzheimer's disease brain and CSF yields putative biomarkers and insights into disease pathways. J. Alzheimer's Dis. **14**:27–41.
8. **Cullen BR.** 2011. Viruses and microRNAs: RISCy interactions with serious consequences. Genes Dev. **25**:1881–1894.
9. **Enright AJ, et al.** 2003. MicroRNA targets in *Drosophila*. Genome Biol. **5**:R1.
10. **Fouchier RA, et al.** 2004. Avian influenza A virus (H7N7) associated with human conjunctivitis and a fatal case of acute respiratory distress syndrome. Proc. Natl. Acad. Sci. U. S. A. **101**:1356–1361.
11. **Gan L, Schwengberg S, Denecke B.** 2011. MicroRNA profiling during cardiomyocyte-specific differentiation of murine embryonic stem cells based on two different miRNA array platforms. PLoS One **6**:e25809.
12. **Gilad S, et al.** 2008. Serum microRNAs are promising novel biomarkers. PLoS One **3**:e3148.
13. **Ginsberg D.** 2002. E2F1 pathways to apoptosis. FEBS Lett. **529**:122–125.
14. **Gottwein E, Cullen BR.** 2008. Viral and cellular microRNAs as determinants of viral pathogenesis and immunity. Cell Host Microbe **3**:375–387.
15. **Govorkova EA, Webster RG.** 2010. Combination chemotherapy for influenza. Viruses (Basel) **2**:1510–1529.
16. **Griffiths-Jones S.** 2004. The microRNA registry. Nucleic Acids Res. **32**: D109–D111.

17. **Griffiths-Jones S, Grocock RJ, van Dongen S, Bateman A, Enright AJ.** 2006. miRBase: microRNA sequences, targets and gene nomenclature. Nucleic Acids Res. **34**:D140–D144.
18. **Griffiths-Jones S, Saini HK, van Dongen S, Enright AJ.** 2008. miRBase: tools for microRNA genomics. Nucleic Acids Res. **36**:D154–D158.
19. **He Y, et al.** 2010. Influenza A virus replication induces cell cycle arrest in G_0/G_1 phase. J. Virol. **84**:12832.
20. **Henke JI, et al.** 2008. microRNA-122 stimulates translation of hepatitis C virus RNA. EMBO J. **27**:3300–3310.
21. **Hermeking H.** 2010. The miR-34 family in cancer and apoptosis. Cell Death Differ. **17**:193–199.
22. **Ho BC, et al.** 2011. Enterovirus-induced miR-141 contributes to shutoff of host protein translation by targeting the translation initiation factor eIF4E. Cell Host Microbe **9**:58–69.
23. **Horimoto T, Nakayama K, Smeekens SP, Kawaoka Y.** 1994. Proprotein-processing endoproteases PC6 and furin both activate hemagglutinin of virulent avian influenza viruses. J. Virol. **68**:6074–6078.
24. **Huang J, et al.** 2007. Cellular microRNAs contribute to HIV-1 latency in resting primary $CD4^+$ T lymphocytes. Nat. Med. **13**:1241–1247.
25. **Huang JC, et al.** 2007. Using expression profiling data to identify human microRNA targets. Nat. Methods **4**:1045–1049.
26. **Huber W, von Heydebreck A, Sultmann H, Poustka A, Vingron M.** 2002. Variance stabilization applied to microarray data calibration and to the quantification of differential expression. Bioinformatics **18**(Suppl 1): S96–S104.
27. **Hummel R, et al.** 2011. Chemotherapy-induced modification of microRNA expression in esophageal cancer. Oncol. Rep. **26**:1011–1017.
28. **Izzotti A, et al.** 2009. Downregulation of microRNA expression in the lungs of rats exposed to cigarette smoke. FASEB J. **23**:806–812.
29. **Jangra RK, Yi M, Lemon SM.** 2010. Regulation of hepatitis C virus translation and infectious virus production by the microRNA miR-122. J. Virol. **84**:6615–6625.
30. **John B, et al.** 2004. Human microRNA targets. PLoS Biol. **2**:e363.
31. **Jopling CL, Schutz S, Sarnow P.** 2008. Position-dependent function for a tandem microRNA miR-122-binding site located in the hepatitis C virus RNA genome. Cell Host Microbe **4**:77–85.
32. **Jopling CL, Yi M, Lancaster AM, Lemon SM, Sarnow P.** 2005. Modulation of hepatitis C virus RNA abundance by a liver-specific MicroRNA. Science **309**:1577–1581.
33. **Kauffmann A, Gentleman R, Huber W.** 2009. arrayQualityMetrics: a bioconductor package for quality assessment of microarray data. Bioinformatics **25**:415–416.
34. **Korteweg C, Gu J.** 2008. Pathology, molecular biology, and pathogenesis of avian influenza A (H5N1) infection in humans. Am. J. Pathol. **172**: 1155–1170.
35. **Lanford RE, et al.** 2010. Therapeutic silencing of microRNA-122 in primates with chronic hepatitis C virus infection. Science **327**:198–201.
36. **Li Y, et al.** 2010. MicroRNA expression and virulence in pandemic influenza virus-infected mice. J. Virol. **84**:3023–3032.
37. **Li Y, et al.** 2011. Differential microRNA expression and virulence of avian, 1918 reassortant, and reconstructed 1918 influenza A viruses. Virology **421**:105–113.
38. **Lim LP, et al.** 2005. Microarray analysis shows that some microRNAs downregulate large numbers of target mRNAs. Nature **433**:769–773.
39. **Lize M, Pilarski S, Dobbelstein M.** 2010. E2F1-inducible microRNA 449a/b suppresses cell proliferation and promotes apoptosis. Cell Death Differ. **17**:452–458.
40. **Lowy RJ.** 2003. Influenza virus induction of apoptosis by intrinsic and extrinsic mechanisms. Int. Rev. Immunol. **22**:425–449.
41. **Luna C, Li G, Qiu J, Epstein DL, Gonzalez P.** 2011. MicroRNA-24 regulates the processing of latent TGFβ1 during cyclic mechanical stress in human trabecular meshwork cells through direct targeting of FURIN. J. Cell Physiol. **226**:1407–1414.
42. **Lyles DS.** 2000. Cytopathogenesis and inhibition of host gene expression by RNA viruses. Microbiol. Mol. Biol. Rev. **64**:709–724.
43. **Lynn DJ, et al.** 2008. InnateDB: facilitating systems-level analyses of the mammalian innate immune response. Mol. Syst. Biol. **4**:218.
44. **Mathivanan S, Fahner CJ, Reid GE, Simpson RJ.** 2012. ExoCarta 2012: database of exosomal proteins, RNA and lipids. Nucleic Acids Res. **40**: D1241–D1244.
45. **Mathivanan S, Ji H, Simpson RJ.** 2010. Exosomes: extracellular organelles important in intercellular communication. J. Proteomics **73**:1907–1920.
46. **Medina RA, Garcia-Sastre A.** 2011. Influenza A viruses: new research developments. Nat. Rev. Microbiol. **9**:590–603.
47. **Nathans R, et al.** 2009. Cellular microRNA and P bodies modulate host-HIV-1 interactions. Mol. Cell **34**:696–709.
48. **Nelson PT, et al.** 2004. Microarray-based, high-throughput gene expression profiling of microRNAs. Nat. Methods **1**:155–161.
49. **Parnell G, et al.** 2011. Aberrant cell cycle and apoptotic changes characterize severe influenza A infection: a meta-analysis of genomic signatures in circulating leukocytes. PLoS One **6**:e17186.
50. **Rager JE, Smeester L, Jaspers I, Sexton KG, Fry RC.** 2011. Epigenetic changes induced by air toxics: formaldehyde exposure alters miRNA expression profiles in human lung cells. Environ. Health Perspect. **119**:494–500.
51. **Schmidt WM, Spiel AO, Jilma B, Wolzt M, Muller M.** 2009. In vivo profile of the human leukocyte microRNA response to endotoxemia. Biochem. Biophys. Res. Commun. **380**:437–441.
52. **Shannon P, et al.** 2003. Cytoscape: a software environment for integrated models of biomolecular interaction networks. Genome Res. **13**:2498–2504.
53. **Silverman JM, Reiner NE.** 2011. Exosomes and other microvesicles in infection biology: organelles with unanticipated phenotypes. Cell. Microbiol. **13**:1–9.
54. **Simons M, Raposo G.** 2009. Exosomes: vesicular carriers for intercellular communication. Curr. Opin. Cell Biol. **21**:575–581.
55. **Skalsky RL, Cullen BR.** 2010. Viruses, microRNAs, and host interactions. Annu. Rev. Microbiol. **64**:123–141.
56. **Smyth GK.** 2004. Linear models and empirical Bayes methods for assessing differential expression in microarray experiments. Stat. Applications Genet. Mol. Biol. **3**:Article3.
57. **Spackman E, et al.** 2002. Development of a real-time reverse transcriptase PCR assay for type A influenza virus and the avian H5 and H7 hemagglutinin subtypes. J. Clin. Microbiol. **40**:3256–3260.
58. **Stieneke-Grober A, et al.** 1992. Influenza virus hemagglutinin with multibasic cleavage site is activated by furin, a subtilisin-like endoprotease. EMBO J. **11**:2407–2414.
59. **Team R.** 2009. R: a language and environment for statistical computing. R Foundation for Statistical Computing, Vienna, Austria.
60. **Thomas M, Lieberman J, Lal A.** 2010. Desperately seeking microRNA targets. Nat. Struct. Mol. Biol. **17**:1169–1174.
61. **Vorwerk S, et al.** 2008. Microfluidic-based enzymatic on-chip labeling of miRNAs. Nat. Biotechnol. **25**:142–149.
62. **Weingartl HM, et al.** 2010. Genetic and pathobiologic characterization of pandemic H1N1 2009 influenza viruses from a naturally infected swine herd. J. Virol. **84**:2245–2256.
63. **Yang X, et al.** 2009. miR-449a and miR-449b are direct transcriptional targets of E2F1 and negatively regulate pRb-E2F1 activity through a feedback loop by targeting CDK6 and CDC25A. Genes Dev. **23**:2388–2393.
64. **Yu JM, et al.** 2011. Age-related changes in mesenchymal stem cells derived from rhesus macaque bone marrow. Aging Cell **10**:66–79.
65. **Zimmerman AL, Wu S.** 2011. MicroRNAs, cancer and cancer stem cells. Cancer Lett. **300**:10–19.
66. **Zuckerman V, Wolyniec K, Sionov RV, Haupt S, Haupt Y.** 2009. Tumour suppression by p53: the importance of apoptosis and cellular senescence. J. Pathol. **219**:3–15.